PNAS
www.pnas.org

Supplementary Information for

A seawater throttle on H_2 production in Precambrian serpentinizing systems

Benjamin M. Tutolo, William E. Seyfried, Jr., Nicholas J. Tosca

Corresponding Author: Benjamin M. Tutolo
Email: benjamin.tutolo@ucalgary.ca

This PDF file includes:

- Supplementary Information Text
- Figure S1
- Table S1
- Caption for Dataset S1

Other supplementary materials for this manuscript include the following:

- Dataset S1

www.pnas.org/cgi/doi/10.1073/pnas.1921042117

Supplementary Information Methods

Fe-Oxidation and -Coordination State in Serpentines

Mössbauer measurements on naturally formed serpentine minerals were compiled from the following sources: Malysheva et al. (1); Rozenson et al. (2); Blaauw et al. (3); Nagy-Czabo et al. (4); O'Hanley and Dyar (5); MacKenzie and McGavin (6); O'Hanley and Dyar (7); Fuchs et al. (8); González-Mancera et al. (9); Votyakov et al. (10); Bishop et al. (11); Klein et al. (12); and Evans et al. (13). An additional measurement, performed on National Museum of Natural History lizardite sample R10581 by Anke Neumann (Newcastle University, Newcastle upon Tyne, United Kingdom), is also included. All 205 of these compiled measurements are included in the supporting information (Dataset S1). Some sources specifically focused on single minerals (i.e., lizardite, chrysotile, or antigorite), while others report data from serpentines of largely unconstrained mineralogy. As discussed in the Methods section, lizardite is the dominant serpentine mineral expected to form during the low-temperature serpentinization processes that are the subject of this study, and chrysotile tends to be a more minor, but still relatively common phase. Antigorite, on the other hand, dominantly forms after lizardite during prograde metamorphism, and we therefore exclude the measurements of antigorite (2, 9, 11, 13, 14) from our analysis of the mechanism for Fe^{3+} incorporation in serpentine. Below, we summarize the quality of the remaining data sets.

Numerous compiled measurements were performed specifically on lizardite. Of these, the O'Hanley and Dyar (5) data set is unique in its development of a robust and well-described sampling and data treatment protocol that included microbeam x-ray diffraction identification of lizardite with a wide range of Fe(III)/Fe(tot) and clear identification and removal of contaminant phases such as brucite and magnetite. These attributes suggest that these data are likely more representative of Fe substitution into lizardite than all of the other compiled lizardite measurements. Other compiled measurements on lizardite are likely compromised due to sample preparation (10) (see below), unconstrained mineralogically (12, 13), or limited in number (8). Thus, although all Mössbauer measurements of serpentinites presented in Dataset S1 are consistent with our conclusion that ferri-Tschermaks substitution is the dominant mode of Fe^{3+} incorporation into serpentine, the fit to the lizardite-specific data are likely more representative of the processes occurring during low-temperature serpentinization.

The extensive lizardite data set from the Urals (10) comprises a significant fraction of all the compiled Mössbauer measurements. It is the only one of the collected data sets to suggest the formation of "oxy-serpentine", which, according to the authors, is characterized by substitution of $^{VI}Fe^{3+}$ by $^{IV}Fe^{3+}$ and an accompanying deprotonation of an -OH group in the lizardite structure. Nevertheless, the veracity of the measurements presented by ref. (10) is questionable on the basis of their unique, likely compromising, sample treatment protocol. The authors soaked their serpentinite samples in 20% acetic acid to remove brucite prior to analysis. This procedure likely had the unintended (and unconstrained) effect of partially dissolving the coexisting serpentine, with preferential, rapid release of Mg and Fe over Si. Indeed, ground serpentinite releases ~2.5% of its total Fe after soaking in 1, 2, and 4 M acetic acid at 20°C for just one hour (15). Recent experiments on sepiolite, a similarly structured silicate mineral, confirm that these rapid rates of cation release are also non-stoichiometric (relative to Si) at room temperature, with the net result being a disintegration of the phyllosilicate structure (16). This latter observation suggests that the observation of 'oxy-serpentine' in this data set is likely an artifact of the sample preparation procedure, rather than representing a naturally occurring product of serpentinization. Problematically, neither the duration of the 20% acetic acid soak used by these authors, nor evidence that it was able to preserve the concentration, oxidation, or coordination state of Fe, were given by ref. (10). Moreover, this sample preparation method is in stark contrast with other studies (e.g., ref. (5)), who take extreme precaution to minimize possible oxidation of Fe during sample preparation, including steps such as grinding samples under acetone. For these reasons, we have excluded this data set from our analysis (Fig. 1), although it is still included in Dataset S1.

Several of the compiled data sets focused specifically on chrysotile specimens (3, 4, 6, 7), many of which were sourced from the same asbestos mining localities. Of these, the measurements presented by ref. (3) and ref. (7) and the room-temperature measurement presented by ref. (6) were included in Fig. 1. Several of the compiled data sets (1, 2, 4) were acquired before the establishment of or did not utilize established data processing procedures for serpentine-group

minerals, with the likely result that their proportions of $^{IV}Fe^{3+}$ and $^{VI}Fe^{3+}$ were misinterpreted (see discussion in ref. (5)), although the calculated values of Fe(III)/Fe(tot), which are included in the Dataset S1 are likely still valid. We therefore exclude these data sets from Fig. 1 and accompanying analysis.

Geochemical model formulation

Calculating thermodynamic properties of serpentinite minerals

Thermodynamic properties of lizardite, greenalite, and hisingerite used in this study can be calculated in a straightforward manner using equations and instructions given by Blanc et al. (17). However, the predictions for the end-member ferri-Tschermaks-substituted serpentines at the heart of this study, Mg-cronstedtite and cronstedtite, are somewhat more complicated and are therefore explicitly outlined here.

Thermodynamic properties of cronstedtite provided by Blanc et al. (17) were estimated by employing the well-constrained properties of tetrahedral Al^{3+} and the $\Delta S^\circ_r = 0$ assumption to substitute $^{[IV]}Fe^{3+}$ for $^{[IV]}Al^{3+}$. Because this technique needed to be used in the present study to calculate a, b, and c for cronstedtite, which are not provided in Blanc et al. (17), it is detailed here. First, the polyhedral model is used to provide an estimate for the hypothetical cronstedtite containing tetrahedrally coordinated Al ($^{[IV]}Al$), i.e., $(Fe^{2+})_2{}^{[VI]}Fe^{3+}(Si,Al)O_5(OH)_4$, according to:

$$S^\circ_{[IV]\,Al\ cronstedtite} = 0.571\ S^\circ_{Fe(OH)_3} + 1.143 + S^\circ_{Fe(OH)_2} + 0.857\ S^\circ_{[VI]FeO} + 0.214\ S^\circ_{[VI]Fe_2O_3} + 0.5\ S^\circ_{[IV]Al_2O_3} + S^\circ_{[IV]SiO_2}\ ,$$

which yields

$$S^\circ_{[IV]Al\ cronstedtite} = 271.31\ \text{J/mol·K}\ .$$

Then, assuming $\Delta S_r^\circ = 0$ J/mol·K, $S^\circ_{cronstedtite}$ may be calculated according to:

$$(Fe^{2+})_2Fe^{3+}(Si,Al)O_5(OH)_4 + 0.5\ {}^{[IV]}Fe_2O_3 = (Fe^{2+})_2Fe^{3+}\ (Si,Fe)O_5(OH)_4 + 0.5\ {}^{[IV]}Al_2O_3\ .$$

Assuming that S° ($^{[IV]}Fe_2O_3$) = S° ($^{[VI]}Fe_2O_3$) = 0 J/mol·K and S° ($^{[IV]}Al_2O_3$) = 29.42 J/mol·K yields $S^\circ_{cronstedtite}$, where cronstedtite is $(Fe^{2+})_2Fe^{3+}(Si,Fe)O_5(OH)_4$, = 256.60 J/mol·K, which is the value reported by Blanc et al. (17). Because $^{[IV]}Al^{3+}$ is a common component of many experimentally constrained phyllosilicate minerals (e.g., muscovite), this technique was determined by Blanc et al. (17) to give more accurate results than using their poorly-constrained empirical correlation for predicting the thermodynamic properties of $^{[IV]}Fe^{3+}$ (17). A similar approach, except with $^{[IV]}Al^{3+}$ and $^{[VI]}Al^{3+}$ substituted for all Fe^{3+} in the hypothetical mineral was used by Helgeson et al. (18). This calculation assumes that the entropy change of the hypothetical Al-cronstedtite ⇌ cronstedtite reaction is zero, which has been shown to be a reasonable approximation (17, 18). Thermodynamic properties for end-member Mg-cronstedtite ($Mg_2Fe^{3+}Fe^{3+}SiO_5(OH)_4$) may then be calculated from the properties of cronstedtite ($Fe_2Fe^{3+}Fe^{3+}SiO_5\ (OH)_4$) according to:

$$\Xi^\circ_{cronstedtite} + 0.857\ \Xi^\circ_{MgO} + 1.143\ \Xi^\circ_{Mg(OH)_2} = \Xi^\circ_{Mg\text{-}cronstedtite} + 0.857\ \Xi^\circ_{FeO} + 1.143\ \Xi^\circ_{Fe(OH)_2}$$

where Ξ° represents V°, S°, C°_p, *a*, *b,* or *c* and the stoichiometric values are calculated according to the number of OH and O bonds in each crystallographic site of the mineral.

The thermodynamic properties for the minerals greenalite, hisingerite, lizardite, cronstedtite, Mg-cronstedtite, Fe^{2+}-serpentine$_{(XMg=0.9)}$ and Fe-brucite used in the geochemical modeling portions of this study are given in Table S1. Consistent with Blanc et al. (17), values of V°, S°, C°_p, *a, b,* and *c* for individual serpentine formulas (i.e., those used for calculating the lines in Fig. 4) are calculated by multiplying the values of individual end-members (i.e., greenalite, lizardite, and/or Mg-cronstedtite) by their end-member contribution to the serpentine solid-solution. Values of ΔH°_f are calculated directly from the equations in Blanc et al. (17), and ΔG°_f can be calculated from ΔH°_f and S° and the expression:

$$\Delta G^\circ_f = \Delta H^\circ_f - T\Delta S^\circ_f$$

where $\Delta S°_f$ is the standard entropy of formation from the elements, whose properties were taken in this study from the CODATA tables (19).

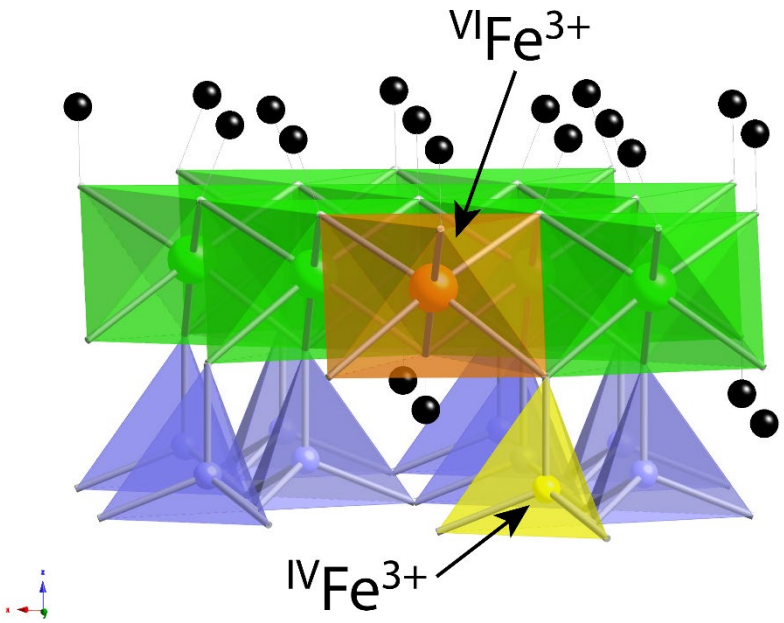

Fig. S1. Lizardite crystal structure model illustrating the operation of the ferri-Tschermaks substitution mechanism. The substitution of $^{IV}Fe^{3+}$ for Si (shown in blue) is illustrated by the yellow atom, and the substitution of $^{VI}Fe^{3+}$ for Mg (shown in green) is illustrated by the orange atom.

Table S1 Thermodynamic properties of minerals employed in this study.

Name	Formula	ΔG°f (kJ/mol)	ΔH°f (kJ/mol)	S° (J/mol/K)	V° (cm^3/mol)	a (J/mol/K)	b (J/mol/K^2)	c (J·K/mol)	Reference
Lizardite	$Mg_3Si_2O_5(OH)_4$	-4037.80	-4365.20	222.01	107.79	303.95	154.34	-70.70	(17)
Greenalite	$Fe_3Si_2O_5(OH)_4$	-2996.53	-3298.40	291.56	105.21	291.23	203.19	-47.53	(17)
Cronstedtite	$Fe^{2+}_2Fe^{+3}_2SiO_5(OH)_4$	-2599.70	-2914.55	313.16	76.80	435.94	106.61	-140.96	(17); a,b,c -This study
Mg-Cronstedtite	$Mg_2Fe^{+3}_2SiO_5(OH)_4$	-3283.07	-3608.49	276.44	83.66	440.15	78.07	-154.23	This study
Fe^{2+}-serpentine$_{(XMg=0.9)}$	$Mg_{2.7}Fe^{+2}_{0.3}Si_2O_5(OH)_4$	-3932.16	-4257.02	228.97	107.53	302.68	159.23	-68.38	This study
Hisingerite	$Fe_2Si_2O_5(OH)_4$	-2941.11	-3220.41	340.01	89.45	273.77	811.39	-220.75	(17, 20)
Fe-Brucite	$Fe(OH)_2$	-492.82		88.00		109.06	18.19	-22.52	(21)

Dataset S1 (separate file). Compiled Mössbauer analyses on serpentines and serpentinites.

Supplement References

1. T. V. Malysheva, V. I. Grachev, I. S. Chashchukhin, Study of Ural serpentines by Mossbauer spectroscopy. *Geokhimiya* **4**, 612–625 (1976).
2. I. Rozenson, E. R. Bauminger, L. Heller-Kallai, Mossbauer spectra of iron in l : l phyllosilicates. *Am. Mineral.* **64**, 893–901 (1979).
3. C. Blaauw, G. Stroink, W. Leiper, Mössbauer analysis of some Canadian chrysotiles. *Can. Mineral.* **17**, 713–717 (1979).
4. I. Nagy-Czabo, *et al.*, ^{57}Fe Mossbauer analysis of chrysotile asbestos from various mining regions. *Acta Geol. Acad. Sci. Hungaricae* **24**, 149–155 (1981).
5. D. S. O'Hanley, M. D. Dyar, The composition of lizardite 1T and the formation of magnetite in serpentinites. *Am. Mineral.* **78**, 391–404 (1993).
6. K. J. D. MacKenzie, D. G. McGavin, Thermal and Mössbauer studies of iron-containing hydrous silicates. Part 8. Chrysotile. *Thermochim. Acta* **244**, 205–221 (1994).
7. D. S. O'Hanley, M. D. Dyar, The composition of chrysotile and its relationship with lizardite. *Can. Mineral.* **36**, 727–739 (1998).
8. Y. Fuchs, J. Linares, M. Mellini, Mossbauer and infrared spectrometry of lizardite-1T from Monte Fico, Elba. *Phys. Chem. Miner.* **26**, 111–115 (1998).
9. G. González-Mancera, F. Ortega-Gutiérrez, N. E. Nava, H. S. Arriola, Mössbauer study of serpentine minerals in the ultramafic body of Tehuitzingo, Southern Mexico. *Hyperfine Interact.* **148**–**149**, 61–71 (2003).
10. S. L. Votyakov, I. S. Chashchukhin, O. L. Galakhova, T. Y. Gulyaeva, Crystal chemistry of lizardite as an indicator of early serpentinization in ultramafic rocks. I. Compositional and structural features of the mineral according to spectroscopic data. *Geochemistry Int.* **43**, 862–880 (2005).
11. J. L. Bishop, M. D. Dyar, E. C. Sklute, A. Drief, Physical alteration of antigorite: a Mössbauer spectroscopy, reflectance spectroscopy and TEM study with applications to Mars. *Clay Miner.* **43**, 55–67 (2008).
12. F. Klein, *et al.*, Iron partitioning and hydrogen generation during serpentinization of abyssal peridotites from 15°N on the Mid-Atlantic Ridge. *Geochim. Cosmochim. Acta* **73**, 6868–6893 (2009).
13. B. W. Evans, M. D. Dyar, S. M. Kuehner, Implications of ferrous and ferric iron in antigorite. *Am. Mineral.* **97**, 184–196 (2012).
14. M. Mellini, Y. Fuchs, J. Linarès, C. Viti, C. Lemaire, Insights into the antigorite structure from Mössbauer and FTIR spectroscopies. *Eur. J. Mineral.* **14**, 97–104 (2002).
15. S. Teir, H. Revitzer, S. Eloneva, C. J. Fogelholm, R. Zevenhoven, Dissolution of natural serpentinite in mineral and organic acids. *Int. J. Miner. Process.* **83**, 36–46 (2007).
16. J. J. P. A. Mulders, E. H. Oelkers, An experimental study of sepiolite dissolution rates and mechanisms at 25 °C. *Geochim. Cosmochim. Acta* **270**, 296–312 (2020).
17. P. Blanc, *et al.*, A generalized model for predicting the thermodynamic properties of clay minerals. *Am. J. Sci.* **315**, 734–780 (2015).
18. H. C. Helgeson, J. M. Delany, H. W. Nesbitt, D. K. Bird, Summary and critique of the thermodynamic properties of the rock-forming minerals. *Am. J. Sci.* **278A**, 229 (1978).
19. V. A. Medvedev, J. D. Cox, D. D. Wagman, *CODATA key values for thermodynamics* (Hemisphere Publishing Corporation New York, 1989).
20. B. M. Tutolo, B. W. Evans, S. M. Kuehner, Serpentine–hisingerite solid solution in altered ferroan peridotite and Olivine Gabbro. *Minerals* **9**, 47 (2019).
21. T. M. McCollom, W. Bach, Thermodynamic constraints on hydrogen generation during serpentinization of ultramafic rocks. *Geochim. Cosmochim. Acta* **73**, 856–875 (2009).